Differences Research in Time Comparison and Positioning of BDS-3 PPP-B2b Signal Broadcast Through GEO

Hongjiao Ma , Jinming Yang , Xiaolong Guan , Jianfeng Wu , Huabing Wu *

Posted Date: 21 May 2025

doi: 10.20944/preprints202505.1665.v1

Keywords: BDS-3; PPP-B2b; time comparison; positioning

 doi:10.20944/preprints202505.1665.v1

Article

Differences Research in Time Comparison and Positioning of BDS-3 PPP-B2b Signal Broadcast Through GEO

Hongjiao Ma [1,3], Jinming Yang [1,2], Xiaolong Guan [1,2], Jianfeng Wu [1,3] and Huabing Wu [1,3,*]

[1] National Time Service Center, Chinese Academy of Sciences, Xi'an 710600, China; mahj@ntsc.ac.cn (H.M.); yangjinming@ntsc.ac.cn (J.M.); guanxl@ntsc.ac.cn (X.G.); wujianf@ntsc.ac.cn (J.F.); whb@ntsc.ac.cn (H.W.)

[2] University of Chinese Academy of Sciences, Beijing 100049, China

[3] Key Laboratory of Time Reference and Applications, Chinese Academy of Sciences, Xi'an 710600, China

* Correspondence: whb@ntsc.ac.cn

Abstract: Three stations in the Asia-Pacific region are selected to form two time comparison links. By comparing the correction accuracy of the satellite orbits and clock deviations of the PPP-B2b messages broadcast by the two GEO satellites of BDS-3 C59 and C61, and taking the time comparison results obtained by the GBM post-ephemeris as a reference, the accuracy of the time comparison of the PPP-B2b messages broadcast by the two GEO satellites C59 and C61 was evaluated. The results show that the accuracy of time comparison between C59 and C61 is similar, but the stability and availability of C59 are better than those of C61. In addition, five IGS/IGMAS stations were selected to evaluate the accuracy of the PPP-B2b message transmitted by the C59 and C61 GEO satellites for BDS-3 positioning, using the IGS/IGMAS weekly solution positioning results as a reference. The results show that the static positioning of PPP-B2b broadcasted by C59 and C61 can reach centimeter level, and the simulated kinematic positioning can reach decimeter level. The positioning accuracy of C59 is higher than that of C61.

Keywords: BDS-3; PPP-B2b; time comparison; positioning

1. Introduction

BDS-3 was officially completed in 2020, and its GEO satellite broadcasts PPP-B2b signals in real time [1-8], and uses the satellite information carried in PPP-B2b messages to correct the satellite orbit and clock deviation, which can achieve more accurate precision single-point positioning and timing. Initially, the same PPP-B2b information will be broadcast synchronously by C59 and C60 satellites. After the second half of 2023, the C61 satellite will be added, and the message content will be different from that broadcast by the previous two GEO satellites. Previous studies have been based on PPP-B2b correction numbers broadcast by C59 and C60 satellites. Xu et al. analyzed the accuracy of PPP-B2b precision tracks in the radial, tangential, and normal directions of 6.8cm, 33.4cm, and 36.6cm, respectively, and the STD of PPP-B2b precision clock deviation reached 0.2ns [9-16]. Tao et al. verified that PPP-B2b signals match 97.5% and 91.5% of BDS-3 and GPS, respectively in the Asia-Pacific region [17]. Sun et al. analyzes the performance of BDS-3 in terms of correction availability, clock and orbit quality and positioning accuracy with PPP-B2b messages[18]. Ren et al. using real-time precise ephemerides are compared against Multi-GNSS Experiment (MGEX) final products and the positioning performance of real-time PPP is evaluated with MGEX/iGMAS stations[19]. Zhang et al. proposed a stable PPP-B2b information matching strategy with broadcast ephemeris [20]. Nie et al. used IGS stations in the Asia Pacific region to verify the centimeter level positioning accuracy of PPP-B2b in both static and dynamic scenarios in three directions [21]. Dai et al. using the observations from six stations spanning 196 days, the long-term positioning performance of BDS-3/GPS real-time PPP with PPP-B2b precise products is evaluated [22]. The average positioning accuracy can be 4.6,

 doi:10.20944/preprints202505.1665.v1

0.9, and 2.5 cm (with a STD of 1.3, 0.7, and 1.7 cm), and 6.4, 3.3, and 9.5 cm (with a STD of 2.3, 1.5, and 3.1 cm) in east, north, and up directions in static and kinematic modes, respectively.

This article compares the differences and similarities between the PPP-B2b correction numbers broadcasted by C59 and C61 satellites, and analyzes the time comparison accuracy of PPP-B2b. Meanwhile, the positioning accuracy of PPP-B2b is studied in terms of static and simulated kinematic positioning.

2. Correction Analysis

2.1. PPP-B2b Correction Accuracy Analysis

The precision clock error and precision orbit of the PPP-B2b correction were restored on March 22, 2024 using the PPP-B2b correction information, and the accuracy of the satellite orbit and clock error after PPP-B2b correction was evaluated by using the GBM precision orbit and precision clock error as a reference. The code deviation products released by the Chinese Academy of Sciences were used as a reference to evaluate the accuracy of the code deviation products in PPP-B2b information. Previous studies have mainly used signals broadcast by C59 and C60 satellites, both of which have the same information content. In this paper, the accuracy of PPP-B2b messages of different contents broadcast by C59 and C61 satellites, referred to as C59_PPP-B2b and C61_PPP-B2b, is analyzed and compared.

2.2. PPP-B2b Orbit Accuracy Analysis

2.2.1. Satellite Orbit Error Evaluation Methods

GBM precise orbit points to the center of mass position of the satellite, while PPP-B2b correction points to the phase center position of the satellite. It is necessary to first correct the center of mass position of the satellite to the phase center position before evaluating the orbit accuracy. Here, the igs14.atx file published by IGS is used for phase center correction. Formula (1) is the correction method:

$$\delta X = X_{GBM} - A \cdot \delta X_{PCO} \quad (1)$$

Among them: δX is the satellite orbit error vector; X_{GBM} is the reference orbit vector obtained for GBM products; A is the satellite attitude matrix; δX_{PCO} is correct the vector for satellite PCO.

After synchronizing the satellite orbit to the center position of the satellite phase, the errors between the PPP-B2b correction position and the reference value in the radial, tangential, and normal directions can be calculated. Formula (2) is the calculation method for errors in three directions:

$$\delta O = [e_{radial} \quad e_{along} \quad e_{cross}]^T \cdot \delta X_{GBM-PPP-B2b} \quad (2)$$

Wherein: δO is the radial, tangential and normal error; e is the direction unit vector; $\delta X_{GBM-PPP-B2b}$ is the difference between the GBM satellite orbit and the PPP-B2b satellite orbit.

2.2.2. Satellite Orbit Accuracy Analysis

Taking the GBM precision orbit as a reference, five BDS-3 satellites and five GPS satellites were used to evaluate the orbit accuracy of PPP-B2b recovery satellites. Figure 1, Figure 2 and Figure 3 are the radial, tangential and normal errors of the CNAV1 broadcast ephemeris satellite orbit and the corrected satellite orbit of PPP-B2b broadcast by C59/C61 respectively. Figures 4, 5 and 6 show the results of the LNAV broadcast ephemeris uncorrected and both corrections.

Figures 1 and 4 show the orbital errors that have not been corrected by PPP-B2b, and it is clear that the orbital error sequence will be discontinuous every hour, which is related to the hour-by-hour update of the broadcast ephemeris. Figure 1, Figure 2, Figure 4 and Figure 5 are the corrected orbit error curves of PPP-B2b, which are smoother than those of the uncorrected error curves, indicating

 doi:10.20944/preprints202505.1665.v1

that the PPP-B2b broadcast by C59 and C61 corrects the hourly discontinuity of the orbits in the broadcast ephemeris of CNAV1.

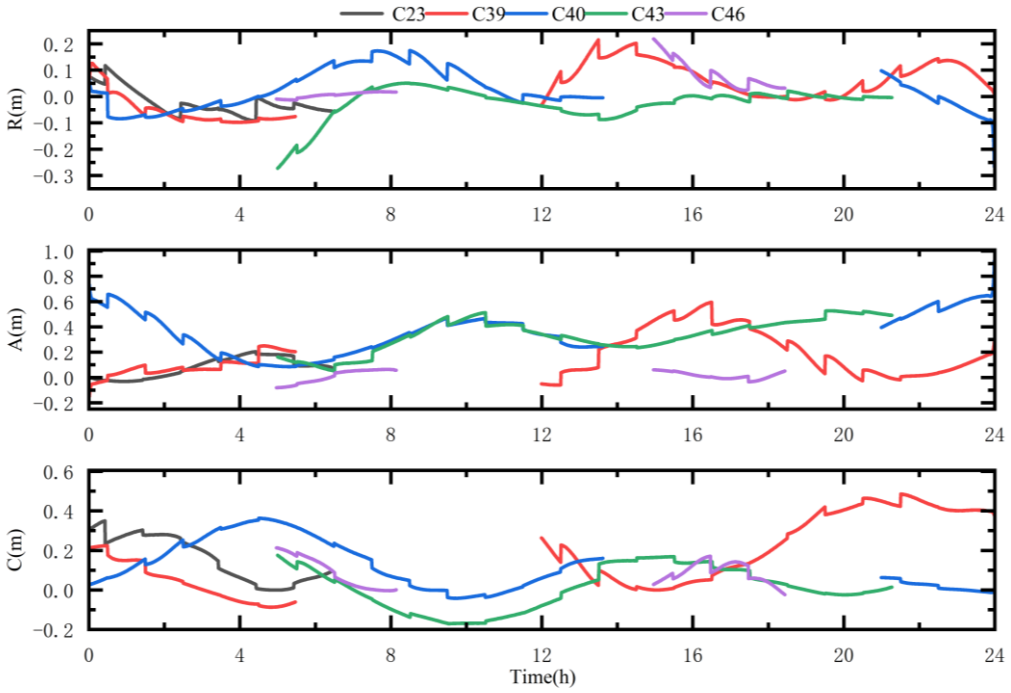

Figure 1. Orbit errors of CNAV1.

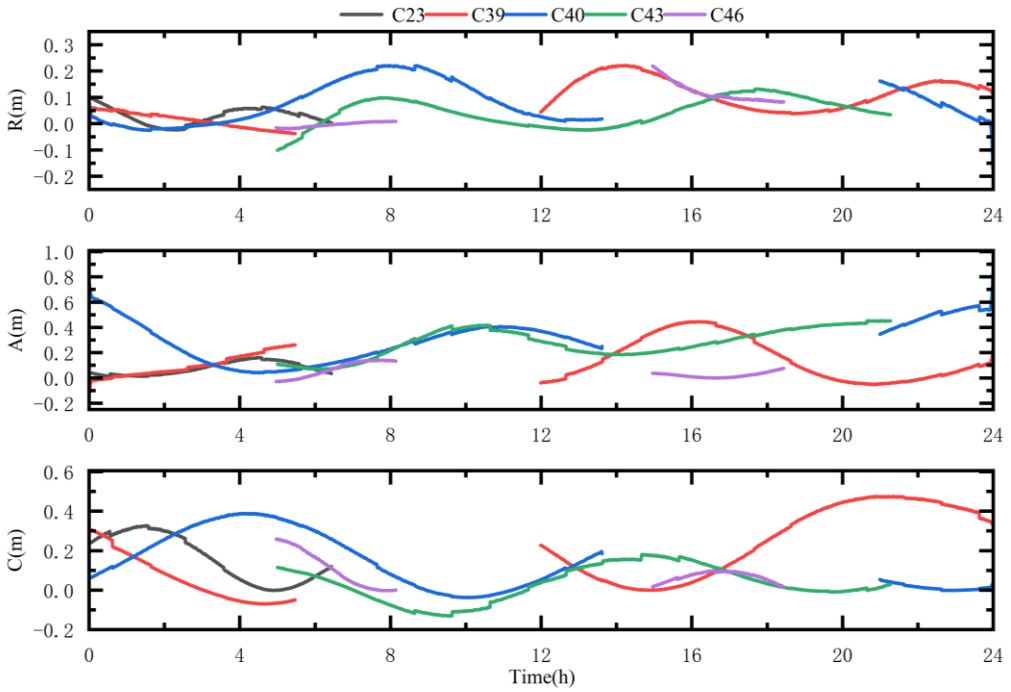

Figure 2. Orbit errors of BDS-3 after C59_PPP-B2b correction.

 doi:10.20944/preprints202505.1665.v1

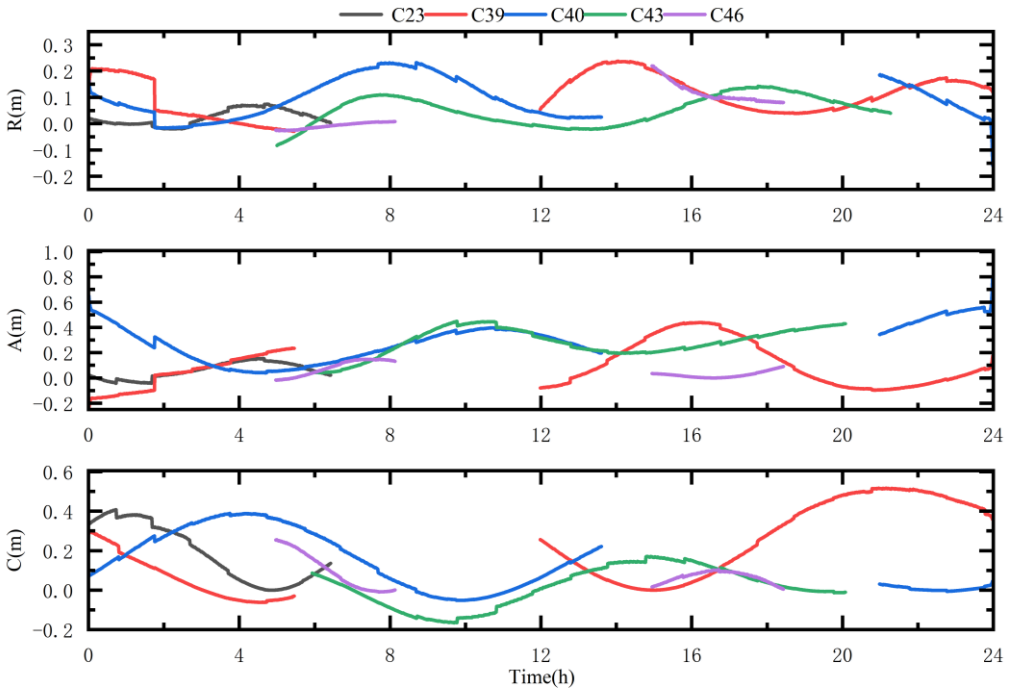

Figure 3. Orbit errors of BDS-3 after C61_PPP-B2b correction.

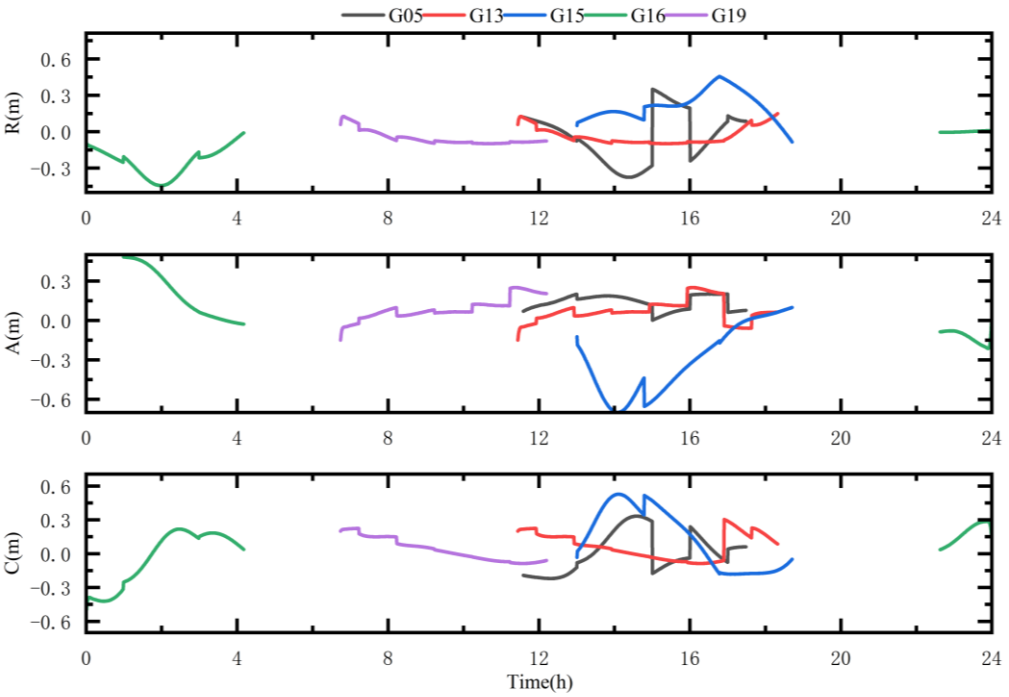

Figure 4. Orbit errors of LNAV.

The variation amplitudes of the orbital error series of BDS-3 in the radial, tangential and normal components are within 0.3, 0.4 and 0.4m respectively. The range of orbit error series of GPS satellites in the three directions is within 0.4, 0.6 and 0.8m respectively. In terms of the magnitude of the change before and after the correction, the correction of the orbit error of the PPP-B2b broadcast by the two GEO satellites is not obvious, so the PPP-B2b mainly corrects the hourly discontinuity of the satellite orbit error.

 doi:10.20944/preprints202505.1665.v1

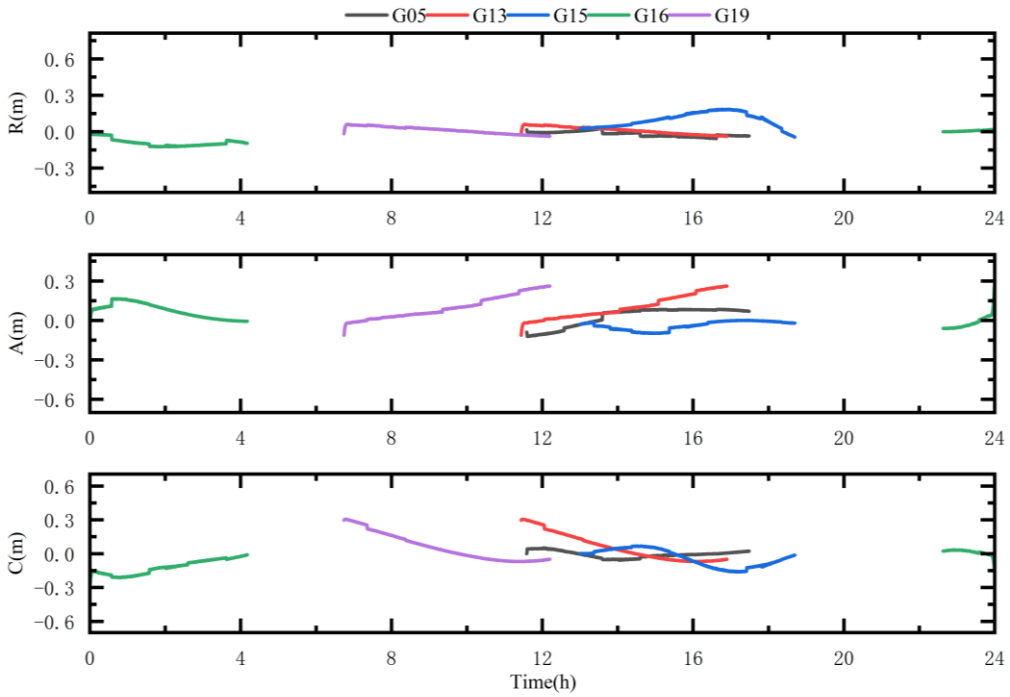

Figure 5. Orbit errors of GPS after C59_PPP-B2b correction.

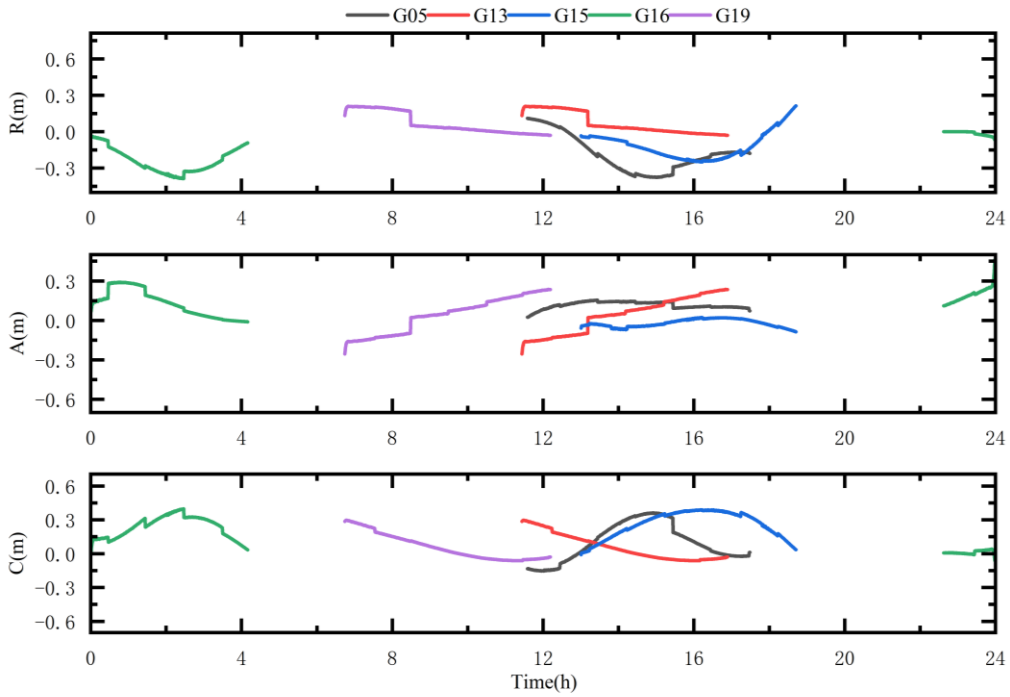

Figure 6. Orbit errors of GPS after C61_PPP-B2b correction.

For the BDS-3 satellite, in terms of the smoothness of the corrected orbits of the two GEO satellites, there is a significant orbital error jump at 2h in Figure 3, while there is no such phenomenon at the same position in Figure 2. Therefore, the correction effect of C59 is slightly better than that of C61.

For GPS satellites, both types of correction information also correct the discontinuity of the orbit every hour. However, from the figure, it can be seen that the correction effect of C59 is slightly better than that of C61. After correction by C61 satellite, there is still a slight discontinuity in the orbit error,

 doi:10.20944/preprints202505.1665.v1

while C59's correction better eliminates this phenomenon. However, compared to the BDS-3 satellite, the error variation of PPP-B2b after correction is smaller, which helps to improve the accuracy of GPS satellite orbit.

In order to further evaluate the satellite orbit accuracy of the PPP-B2b, Table 1 provides the average root mean square error of the broadcast ephemeris orbit and PPP-B2b real-time orbit for seven days from March 22 to March 28, 2024. From the statistical values in the table, it can also be concluded that for BDS-3, both the PPP-B2b correction values broadcasted by C59 and C61 satellites have improved the accuracy of the broadcast ephemeris orbit to a certain extent, and also corrected the discontinuity of the orbit in the broadcast ephemeris, making the error smoother. However, for GPS satellites, the correction values of C59 and C61 have improved the accuracy of radial, normal, and tangential directions, with C59 having a higher correction accuracy.

Table 1. Average RMS of orbit errors.

Items	Radial (cm)	Tangential (cm)	Normal (cm)
BDS-3 CNAV1	8.34	23.05	17.46
BDS-3 C59_PPP-B2b	7.83	20.46	17.16
BDS-3 C61_PPP-B2b	8.14	19.88	18.46
GPS LNAV	15.46	22.49	19.05
GPS C59_PPP-B2b	6.83	9.73	8.94
GPS C61_PPP-B2b	9.86	11.57	15.49

2.3. PPP-B2b Clock Error Accuracy Analysis

2.3.1. Evaluation Method for Satellite Clock Error

Due to the fact that the system time used for GBM precision clock bias is GPST, while the system time used for PPP-B2b is BDT, it is necessary to correct the time difference of 14 seconds between different time systems before evaluating the accuracy of satellite clock bias. For the BDS-3 system, the linear combination of B1I and B3I used by GBM precision clock bias serves as the frequency reference, while PPP-B2b uses B3I frequency as the reference, so code deviation calibration is required for different observed quantities [23-25]. For GPS systems, since PPP-B2b does not broadcast GPS code deviation information, there is no need to unify the frequency reference. Formulas (3) and (4) are specific correction methods:

For BDS-3 system:

$$\delta t = dt_{GBM} - dt_{PPP-B2b} - \frac{f_{B1I}^2}{f_{B1I}^2 - f_{B3I}^2}\mathrm{DCB}_{B1I} \tag{3}$$

For GPS systems:

$$\delta t = dt_{GBM} - dt_{PPP-B2b} \tag{4}$$

Among them: δt is the error of satellite clock bias; dt is the satellite clock bias; f is the signal frequency; DCB_{B1I} is the code deviation between B1I and B3I signals.

2.3.2. Analysis of Satellite Clock Error Accuracy

Using GBM precision clock bias as a reference, evaluate the accuracy of PPP-B2b recovered satellite clock bias for five BDS-3 satellites and five GPS satellites. Figure 7 shows the clock error curve of BDS-3 satellite before and after correction on March 22, 2024. For the BDS-3 satellite, the clock bias error corrected by PPP-B2b broadcasted by C59 and C61 fluctuates within 1ns, while the variation range of satellite clock bias in CNAV1 broadcast ephemeris is within 3ns. At the same time, the hourly discontinuity in the broadcast ephemeris is also eliminated by PPP-B2b. From the curve in the figure, it can be seen that the PPP-B2b broadcasted by C59 and C61 have similar correction effects on clock bias.

 doi:10.20944/preprints202505.1665.v1

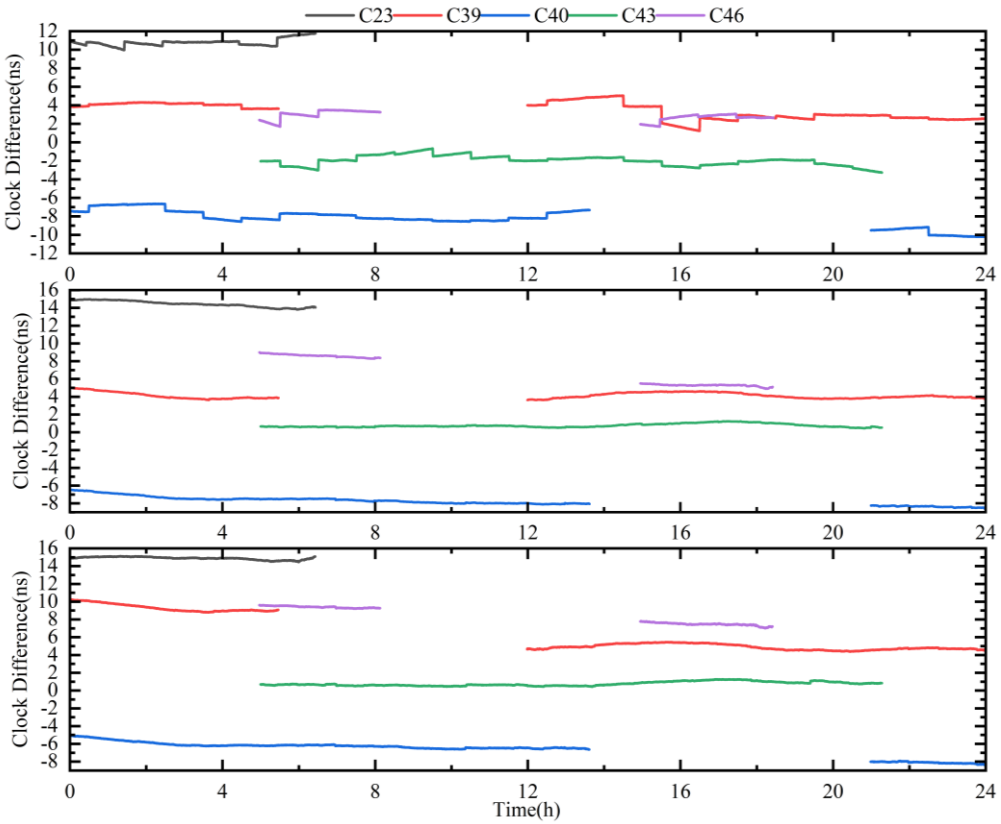

Figure 7. Corrected BDS-3 Clock Bias Errors for CNAV1 and C59_PPP-B2b (Middle) C61_PPP-B2b (Lower).

The situation of GPS satellites is quite unique. From Figure 8, it can be seen that the clock bias error changes more significantly after PPP-B2b correction. However, for G13 and G19 satellites, the discontinuity of clock bias is eliminated because the GPS satellite clock reference was not maintained during the generation of PPP-B2b products.

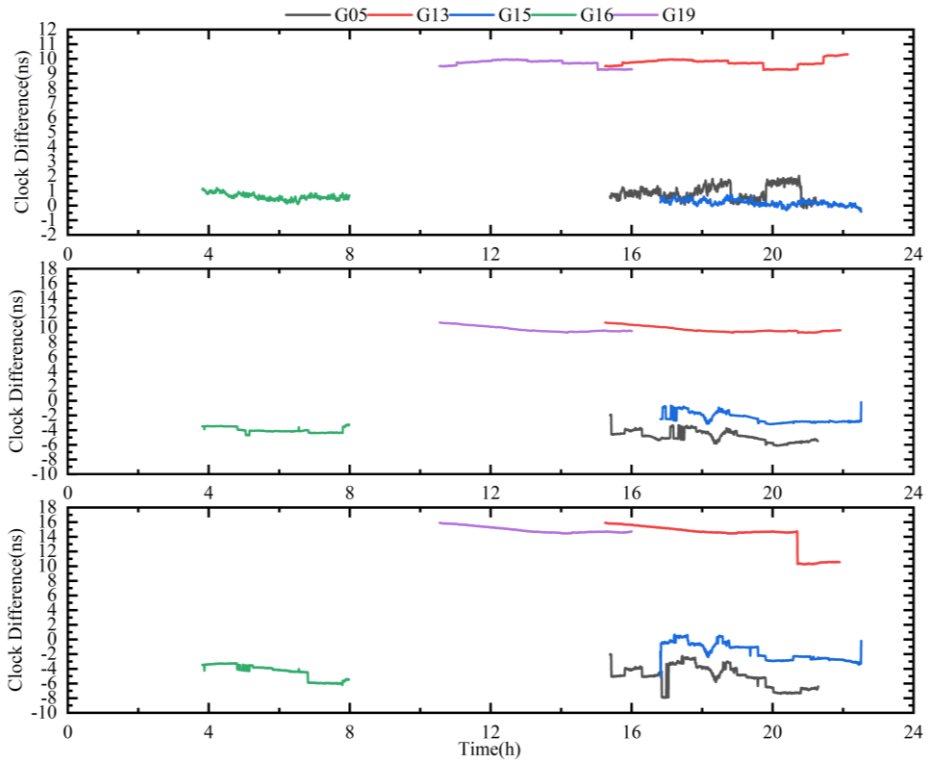

Figure 8. Corrected GPS Clock Bias Errors for LNAV and C59_PPP-B2b (Middle) C61_PPP-B2b (Lower).

 doi:10.20944/preprints202505.1665.v1

However, a single clock bias still exists in the clock bias sequence. In order to effectively evaluate the accuracy of PPP-B2b corrected satellite clock bias, it is necessary to correct individual clock offset deviations by subtracting the average clock offset [26]. For example, the real-time PPP-B2b clock deviation of C23 satellite reaches 10ns. Research has shown that the systematic errors unique to these satellites are related to pseudorange observations. If carrier phase observation is used for positioning, the system error specified by the satellite can be absorbed by ambiguity.

In order to more intuitively demonstrate the difference in satellite clock bias before and after PPP-B2b correction, Table 2 shows the clock bias STD obtained by BDS-3 and GPS systems from broadcast messages and PPP-B2b for a total of 7 days from March 22 to March 28, 2024. From the table, it can be seen that the clock error accuracy of BDS-3 satellite has significantly improved after PPP-B2b correction, but the PPP-B2b correction effect broadcasted by C59 satellite is better; However, PPP-B2b did not improve the clock bias accuracy of GPS satellites, and the corrected accuracy of PPP-B2b broadcasted by C61 satellite was worse than that of C59.

Table 2. Average RMS of clock difference errors.

Items	STD (ns)
BDS-3 CNAV1	0.64
BDS-3 C59_PPP-B2b	0.22
BDS-3 C61_PPP-B2b	0.24
GPS LNAV	0.31
GPS C59_PPP-B2b	0.61

2.3.3. PPP-B2b Code Deviation Accuracy

After comparison, it was found that, the inter symbol deviation correction values in PPP-B2b broadcasted by two GEO satellites, C59 and C61, are the same. Figure 9 and Figure 10 compare the satellite code deviation published by the Chinese Academy of Sciences with the code deviation real-time broadcast by PPP-B2b from March 22 to March 28, 2024. The frequency of comparison is respectively B1C (P) [27] and B3I and B1I and B3I. Since PPP-B2b currently only broadcasts the code deviation of BDS-3 satellite, this part is only for BDS-3 satellite.

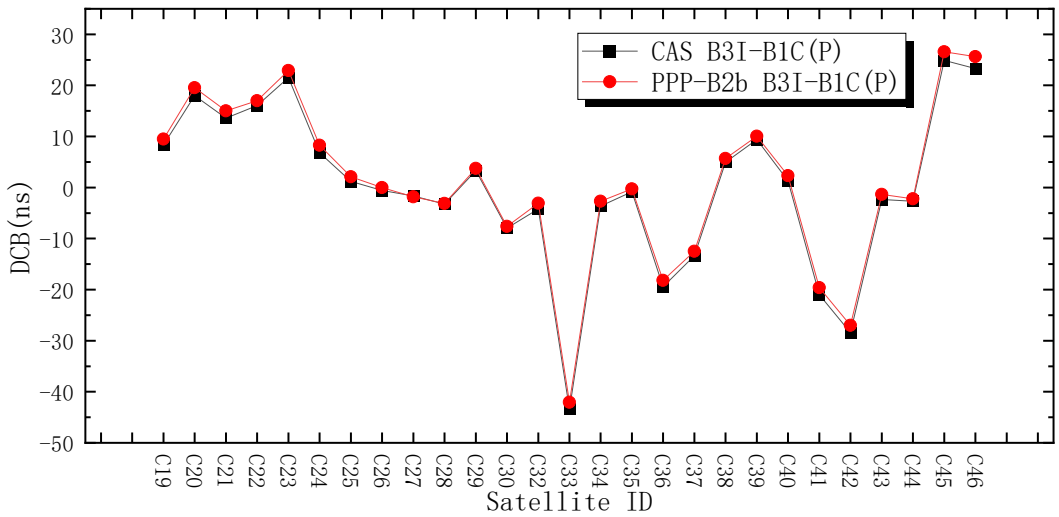

Figure 9. Code bias between B1C(P) and B3I.

 doi:10.20944/preprints202505.1665.v1

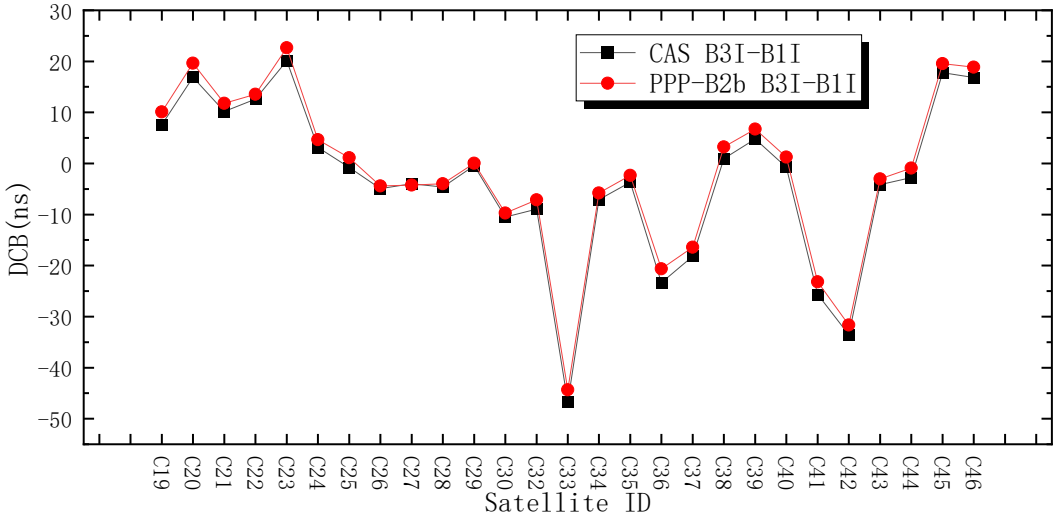

Figure 10. Code bias between B1I and B3I.

From the two figures, it can be seen that the code deviations of PPP-B2b and CAS are consistent, and the systematic deviation is very small. For the deviation between B1C (P) and B3I, the difference STD between PPP-B2b and CAS is 0.535ns, and for B1I and B3I, the difference STD is 0.763ns, which is similar to satellite clock bias. Due to the large weight of carrier phase observations used for precise single point positioning, systematic errors can be absorbed by ambiguity [28].

3. PPP-B2b Time Comparison

3.1. PPP-B2b Time Comparison Processing Strategy

A time comparison study of BDS-3 B1I/B3I+GPS L1/L2 ionosphere free combination was conducted using BDS-3 PPP-B2b. The Sinan K803 receiver was used to receive and save the original binary message of PPP-B2b broadcasted by GEO satellite from March 22 to March 28, 2024, and decode the binary message according to the "Precision Single Point Positioning Service Signal PPP-B2b" file. The research adopts the receiver observation data of XIA6, SE22 and JLJI stations of the National Time Service Center of the Chinese Academy of Sciences [29]. Table 3 shows the information of GNSS receivers participating in the PPP-B2b time comparison. XIA6 and SE22 are GNSS receiver stations with a common atomic clock and antenna in the NTSC laboratory. XIA6 and SE22 are both connected to the local UTC (NTSC), and JLJI is externally connected to the local hydrogen clock.

The experimental design first uses the BDS-3+GPS dual system for zero baseline time comparison to verify the correctness of the PPP-B2b time comparison proposed in the previous section, and then uses the GBM post precision product as a reference for experimental analysis of long baseline time comparison.

Table 3. Station information of PPP-B2b time transfer.

Station name	Station category	Receiver model	Antenna model	external clock
XIA6	NTSC	Sept Polarx5TR	SEPCHOKE_B3E6	UTC(NTSC)
SE22	NTSC	Sept Polarx5TR	SEPCHOKE_B3E6	UTC(NTSC)
JLJI	NTSC	TRIMBLE ALLOY	SEPCHOKE_B3E6	H-MASER

The processing strategy of PPP-B2b is shown in Table 4. The precise satellite position and clock bias are obtained by correcting the satellite position and clock bias calculated through navigation messages using PPP-B2b products. The ionospheric delay uses a dual frequency ionosphere free combination to eliminate ionospheric effects, and the extended Kalman filter is used for parameter estimation. It is a recursive filtering algorithm used to estimate the system state and update and

 doi:10.20944/preprints202505.1665.v1

correct errors based on measurement data. And use igs14.atx to eliminate the deviation between the antenna phase center and centroid.

Table 4. Error terms and processing models of PPP-B2b time transfer.

Error terms	Processing model
Precise ephemeris and clock bias	PPP-B2b Precision Orbit and Clock Error
Ionospheric delay	Dual frequency ionosphere free combination
Tropospheric time delay	ZTD estimation
Observations	B1I/B3I, L1/L2 code pseudorange and carrier phase
Elevation mask	15°
Solid tide correction	IERS 2010
Antenna Phase Center	igs14.atx
Parameter estimation	Extended Kalman Filter
Receiver position model	Static model
Receiver clock bias model	White noise
Observation value sampling interval	30s

3.2. PPP-B2b Time Comparison Analysis

3.2.1. Zero Baseline PPP-B2b Time Comparison

The zero baseline common clock experiment selects the observation data of two external UTC (NTSC) receivers from the National Time Service Center of the Chinese Academy of Sciences. The continuous day zero baseline common clock time comparison can reflect the uncertainty of receiver noise and product time comparison. Figure 11 shows the PPP-B2b time comparison results of zero baseline clock XIA6 and SE22 using BDS-3+GPS. From Figure 11, it can be seen that the time comparison noise of C59_PPP-B2b and C61_PPP-B2b fluctuates within 0.5ns. The STD of the time comparison of C59_PPP-B2b is 0.071ns, and the STD of the time comparison of C61_PPP-B2b is 0.094ns. Due to the automatic calibration of internal delay in XIA6 and the absence of SE22, there is a constant deviation of about 26ns in the PPP-B2b dual frequency ionosphere free combination zero baseline clock time comparison results between the two receivers. From Figure 11, it can be seen that the availability of C61_PPP-B2b is inferior to C59_PPP-B2b in the final time period, which also results in slightly poorer performance of its zero-baseline time transfer STD.

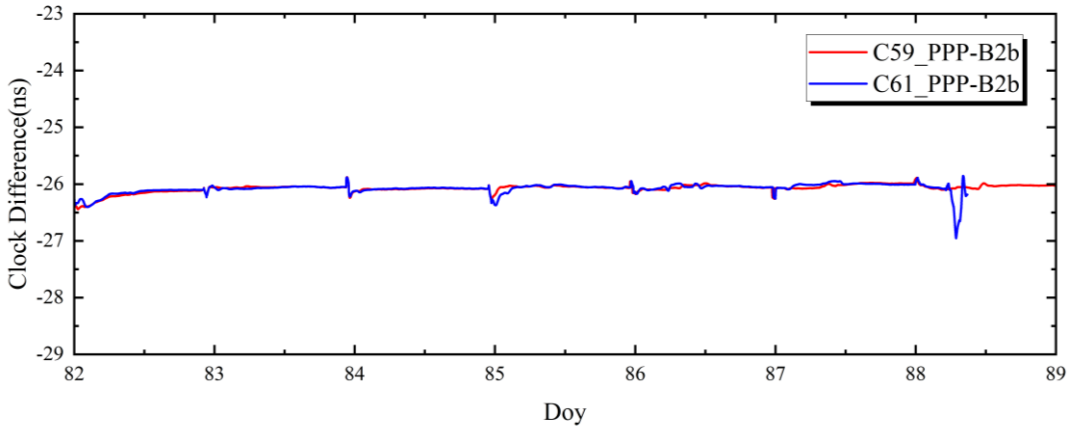

Figure 11. BDS-3+GPS PPP-B2b zero-baseline time transfer.

Figure 12 shows the corrected Allan variances of C59_PPP-B2b and C61_PPP-B2b during zero baseline time transfer, with a high degree of consistency between the two. C59_PPP-B2b is slightly better than C61_PPP-B2b overall. At 1000s, the zero baseline co clock PPP-B2b time comparison of C59_PPP-B2b and C61_PPP-B2b resulted in a corrected Allen variance better than 1E-13. The corrected Allen variances for 100000 seconds reached 3.56E-16 and 3.67E-16, respectively. Thus, the

 doi:10.20944/preprints202505.1665.v1

reliability of PPP-B2b time comparison was verified, providing the possibility for PPP-B2b long baseline time comparison.

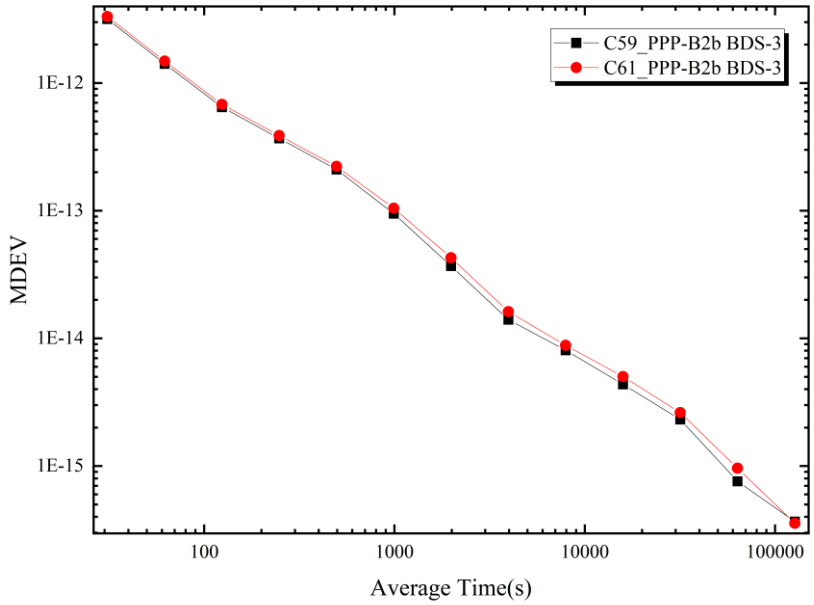

Figure 12. BDS-3+GPS PPP-B2b zero-baseline time transfer MDEV.

3.2.2. Long Baseline PPP-B2b Time Comparison

Figure 13 shows the comparison results of BDS-3+GPS dual system C59_PPP-B2b long baseline time between XIA6 and JLJI stations from March 22 to March 28, 2024. The reference in the figure is the time comparison results of precise single point positioning using GBM's post production BDS-3+GPS dual system. From Figure 13, it can be seen that there is almost no system deviation in the time comparison between the PPP-B2b dual system dual frequency ionosphere free combination and the GBM dual system ionosphere free combination. Subtracting them can more clearly observe the residual of the PPP-B2b time comparison. Figure 14 shows the obtained time difference curve, with time difference fluctuations kept within 2ns, and the STD of time comparison and reference value difference is 0.544ns.

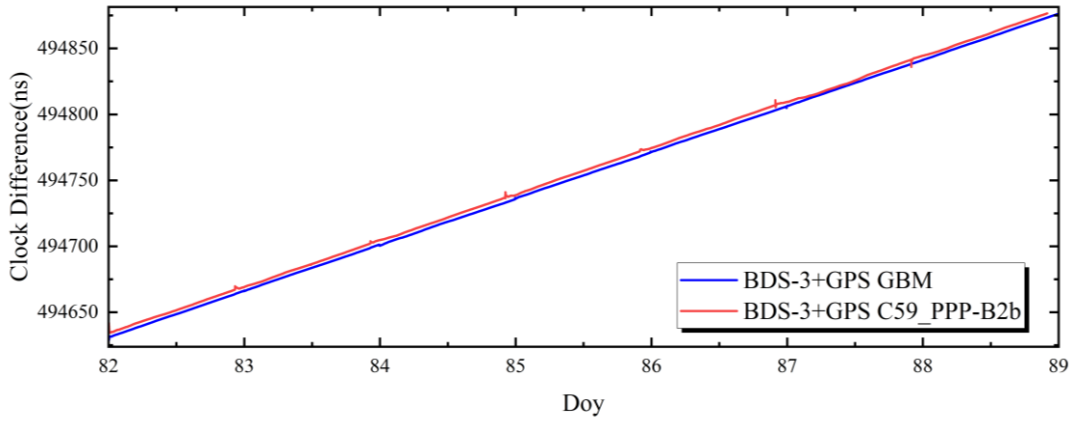

Figure 13. BDS-3+GPS performs XIA6-JLJI time transfer sequence(C59_PPP-B2b).

 doi:10.20944/preprints202505.1665.v1

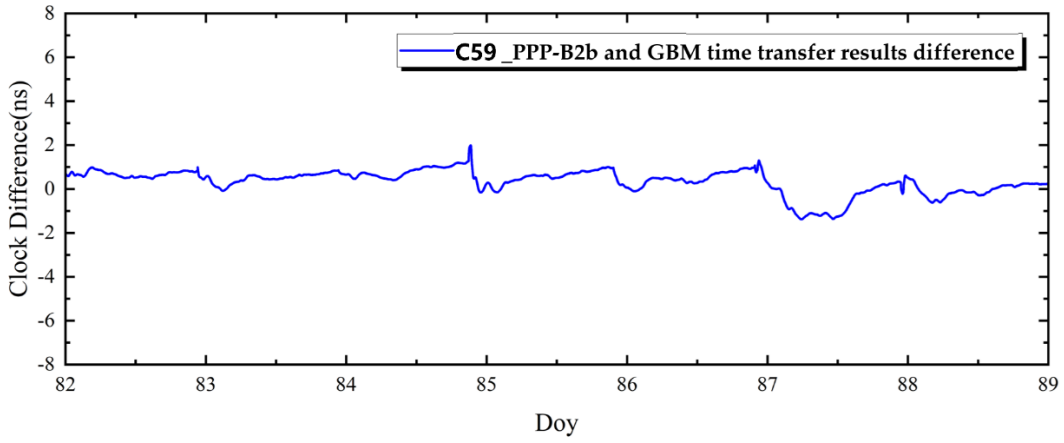

Figure 14. BDS-3+GPS performs XIA6-JLJI time transfer residual sequence(C59_PPP-B2b).

The two curves in Figure 15 represent the corrected Allen variance of the clock bias of the XIA6-JLJI receivers obtained through the BDS-3+GPS PPP-B2b dual frequency ionosphere free combination and the use of GBM products for BDS-3+GPS. From the graph, it can be seen that the stability of GBM time transfer is better than C59_PPP-B2b, but the stability trend of C59_PPP-B2b is the same as GBM. As time increases, the difference in stability between C59_PPP-B2b and GBM gradually decreases. At 10000 seconds, the stability difference between the two is only 2.1E-15. The stability of C59_PPP-B2b in XIA6 and JLJI reached 3.87E-15 with a time comparison of 10000 seconds.

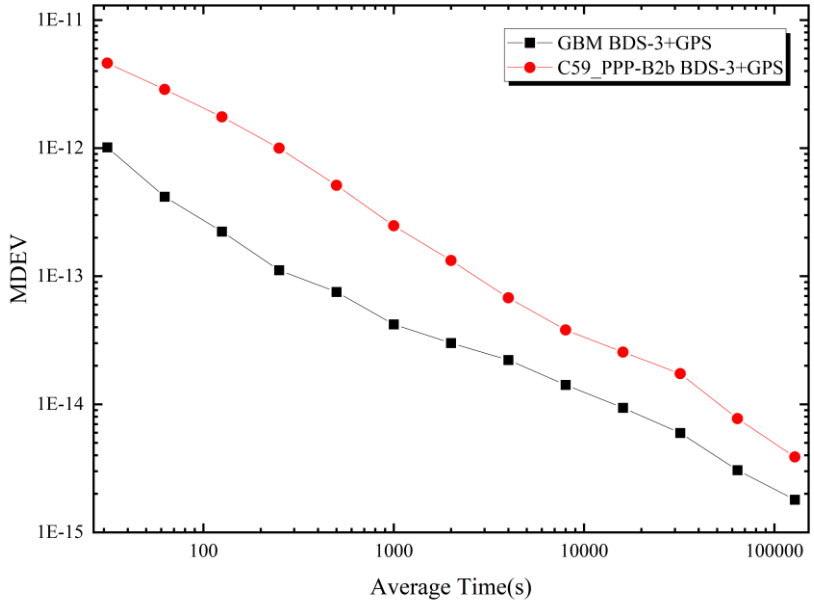

Figure 15. BDS-3+GPS performs XIA6-JLJI time transfer MDEV(C59_PPP-B2b).

Figure 16 shows the comparison results of BDS-3+GPS C61_PPP-B2b long baseline time between XIA6 and JLJI stations from March 22 to March 28, 2024. The reference in the figure is the time comparison results of precise single point positioning using GBM post product BDS-3+GPS. From Figure 16, it can be seen that both curves have no systematic deviation, but there is a gap in the availability of C61_PPP-B2b for a period of time, indicating that there is a certain gap compared to C59_PPP-B2b. Subtracting the two can more clearly observe the residual of C61_PPP-B2b time comparison. Figure 17 shows the obtained time difference curve, and the time difference fluctuation remains within 2ns. The STD of time comparison difference is 0.511ns.

 doi:10.20944/preprints202505.1665.v1

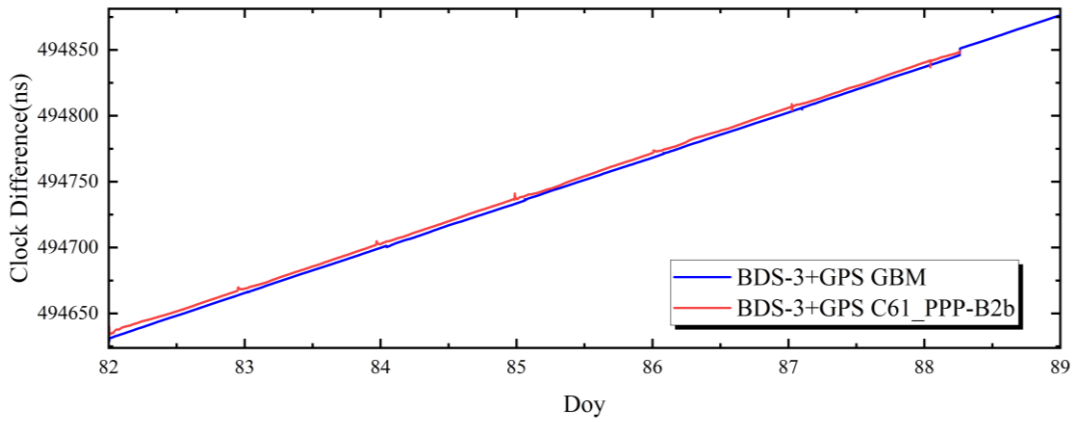

Figure 16. BDS-3+GPS performs XIA6-JLJI time transfer sequence(C61_PPP-B2b).

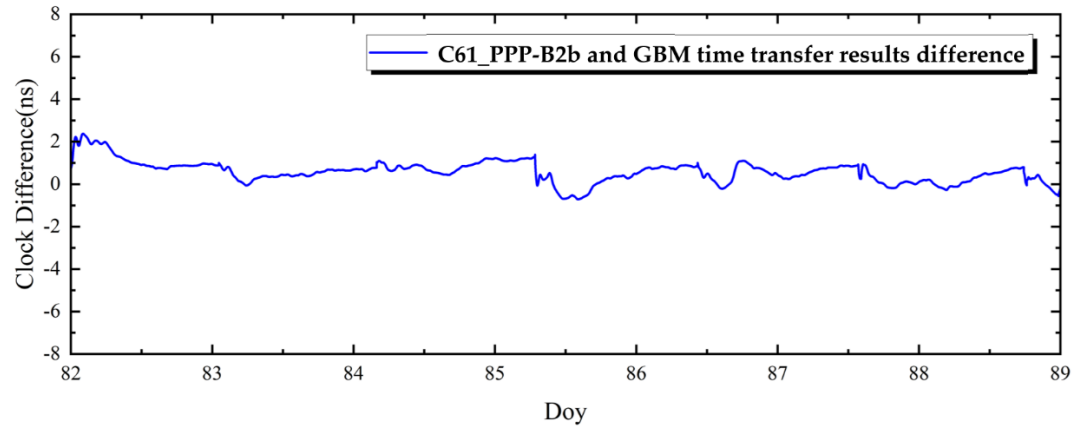

Figure 17. BDS-3+GPS performs XIA6-JLJI time transfer residual sequence(C61_PPP-B2b).

The two curves in Figure 18 represent the corrected Allen variance of the clock bias of the XIA6-JLJI receivers obtained through the BDS-3+GPS PPP-B2b dual frequency ionosphere free combination and the use of GBM products for BDS-3+GPS. From the graph, it can be seen that the overall stability of GBM time transfer is still better than C61_PPP-B2b, and the time difference is relatively large in the short term. With the increase of time, the stable rate of C61_PPP-B2b is higher than that of GBM. At 10000 seconds, the stability difference between the two is only 0.2E-15. The stability of C61_PPP-B2b in XIA6 and JLJI reached 1.99E-15 at a time ratio of 10000 seconds, which is higher than the stability of C59_PPP-B2 at the same time.

 doi:10.20944/preprints202505.1665.v1

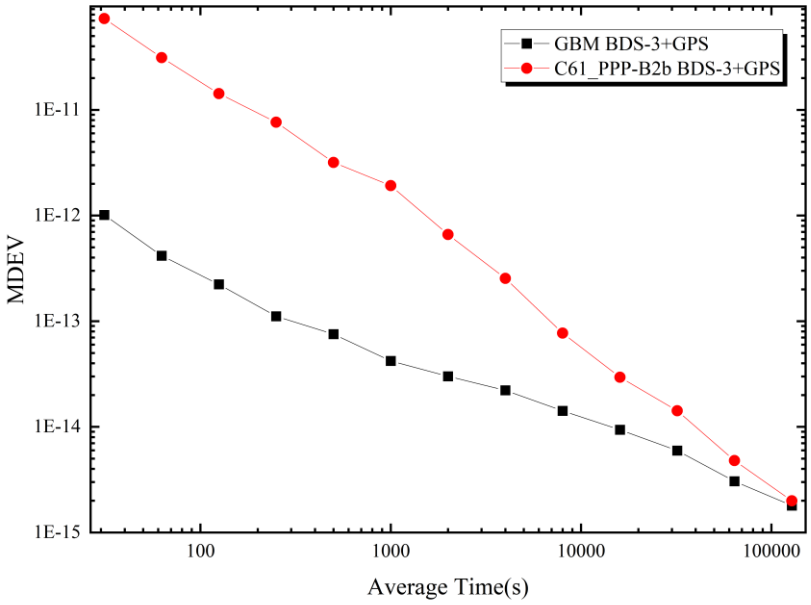

Figure 18. BDS-3+GPS performs XIA6-JLJI time transfer MDEV(C61_PPP-B2b).

3.2.3. Comparison of Time Transfer Links

The BDS-3+GPS combination was used to study the accuracy of time comparison between C59_PPP-B2b and C61_PPP-B2b. Table 5 presents two performance indicators, STD and modified Allan variance, for time comparison between zero baseline and long baseline. From these two indicators, it can be seen that the time comparison accuracy of C59_PPP-B2b and C61_PPP-B2b is close, but the stability and availability of C59_PPP-B2b are better than C61_PPP-B2b.

Table 5. PPP-B2b time transfer accuracy statistics.

Items	PPP-B2b	Time comparison STD (ns)	Correct Allen's variance
XIA6-SE22	C59	0.071	3.56 E-16
	C61	0.094	3.67 E-16
XIA6-JLJI	C59	0.544	3.87 E-15
	C61	0.511	1.99 E-15

4. PPP-B2b Positioning

4.1. PPP-B2b Positioning Processing Strategy

Select 5 IGMAS/IGS observation stations in the Asia Pacific region for precise single point positioning of PPP-B2b based on BDS-3/GPS. The experiment used the BDS-3 B1I/B3I ionosphere free combination and the BDS-3 B1I/B3I+GPS L1/L2 ionosphere free combination to study the PPP-B2b localization of C59 and C61. The detailed information of each experimental station is shown in Table 6.

Table 6. Station information for PPP-B2b positioning research.

Station name	Station category	Receiver model	Antenna model	external clock
GAMG	IGS	Sept Polarx5TR	LEIAR25.R4 LEIT	INTERNAL
GUA1	IGMAS	MGR_iGMAS	Geodetic-GNSS	RUBIDIUM
JFNG	IGS	TRIMBLE ALLOY	TRM59800.00	INTERNAL
SHA1	IGMAS	Unicore UB4B0	NOV750.R4 NOVS	RUBIDIUM
USUD	IGS	Sept Polarx5	AOAD/M_T JPLA	H-MASER

 doi:10.20944/preprints202505.1665.v1

The processing strategy of PPP-B2b is shown in Table 7. The precise satellite position and clock bias are obtained by correcting the satellite position and clock bias calculated through navigation messages using PPP-B2b. The ionospheric delay uses a dual frequency ionosphere free combination to eliminate ionospheric effects, and uses extended Kalman filtering and least squares estimation for parameter estimation. It is a recursive filtering algorithm used to estimate the system state and update and correct errors based on measurement data. Two combinations of static PPP-B2b positioning calculations were performed on a daily basis based on experimental data. Due to the convergence time required for precise single point positioning methods, the solution results corresponding to the convergence time are removed from the daily data involved in positioning.

Table 7. Error terms and processing models of PPP-B2b positioning.

Error terms	Processing model
Precise ephemeris and clock bias	PPP-B2b Precision Orbit and Clock Error
Ionospheric delay	Dual frequency ionosphere free combination
Tropospheric time delay	ZTD estimation
Observations	B1I/B3I, L1/L2 code pseudorange and carrier phase
Elevation mask	15°
Solid tide correction	IERS 2010
Antenna Phase Center	igs14.atx
Parameter estimation	Extended Kalman Filter, least squares estimation
Receiver position model	Constant Model
Receiver clock bias model	White noise
Observation value sampling interval	30s

4.2. BDS-3 PPP-B2b Positioning Research

Figure 19 shows the average number of satellites in the static calculation epoch of the station. The average number of BDS satellites involved in PPP-B2b calculation per epoch for these 5 stations is 7.85. The USUD observation station has the fewest number of satellites among the five stations, which also leads to poorer positioning performance of PPP-B2b.

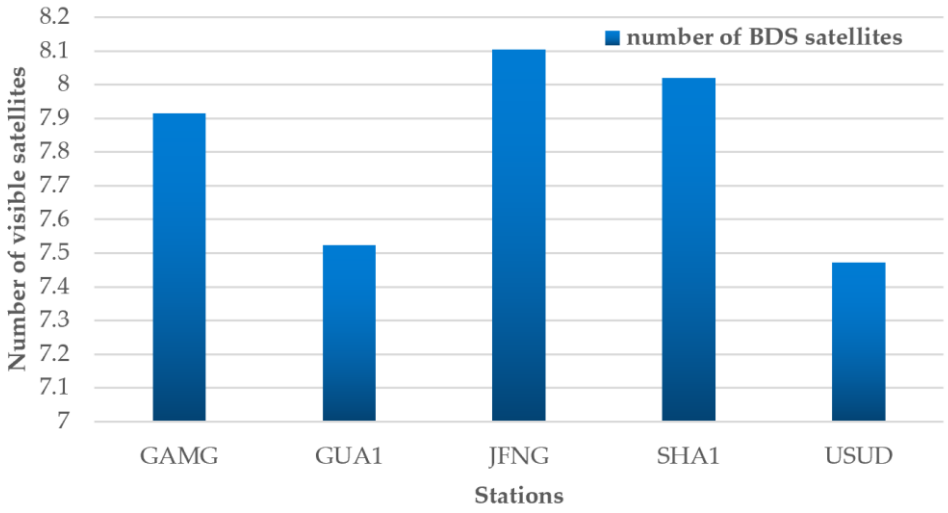

Figure 19. Number of visible satellites in BDS-3.

4.2.1. BDS-3 PPP-B2b Static Positioning

Taking the GAMG station on March 22, 2024 as an example, Figures 20 and 21 show the results of static positioning in the East North Up (E/N/U) direction over time. The E/N/U direction error sequences from top to bottom represent the positioning of PPP-B2b broadcasted by C59 satellite and

 doi:10.20944/preprints202505.1665.v1

C59 satellite, respectively. In order to more intuitively see the convergence effect, the image omits half an hour of convergence process. The RMS errors in the E/N/U direction after static positioning convergence of C59-PPP-B2b are calculated to be 3.21/1.37/4.47 cm, and the RMS errors in the E/N/U direction for C61_PPP-B2b are 4.43/1.95/5.49 cm, respectively. GAMG stands at the static PPP-B2b positioning convergence point, and the static positioning errors of C59-PPP-B2b and C61_PPP-B2b fluctuate within 0.03 meters.

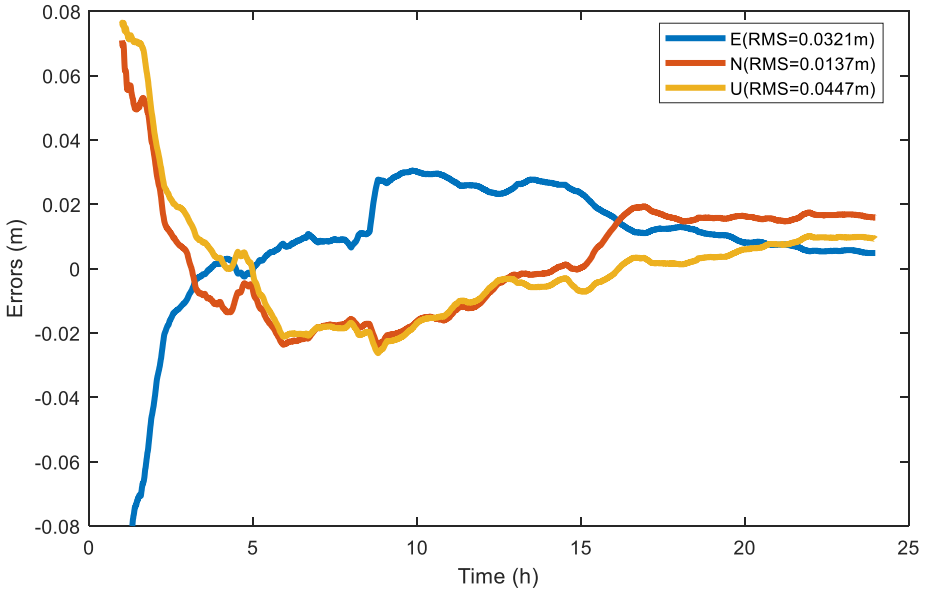

Figure 20. GAMG station BDS-3 C59_PPP-B2b static positioning results.

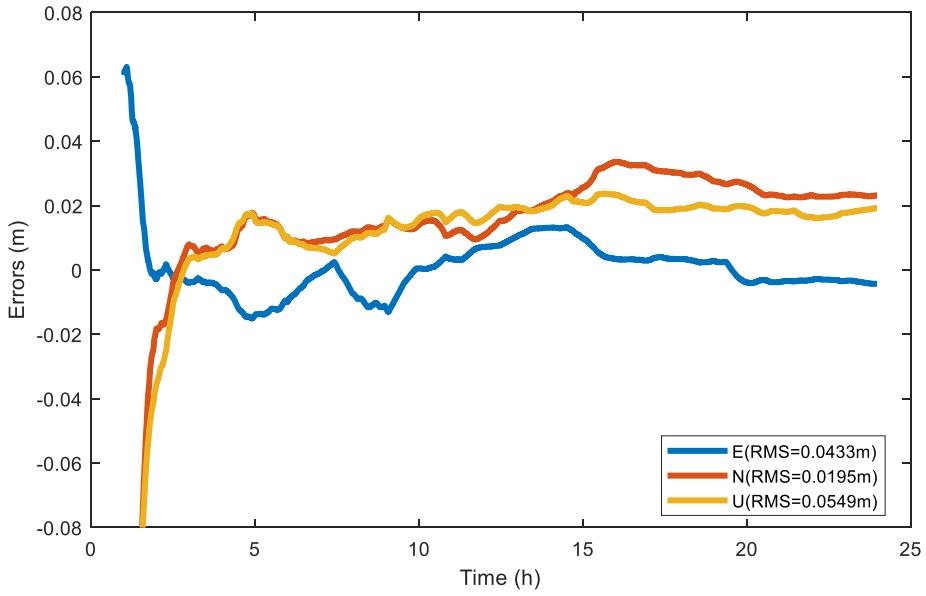

Figure 21. GAMG station BDS-3 C61_PPP-B2b static positioning results.

Figure 22 shows the variation of the number of satellites and the positioning accuracy factor (PDOP) over time during BDS-3 PPP-B2b positioning by GAMG station on March 22, 2024. The average number of visible satellites for precise single point positioning calculation is around 8, and the position accuracy factor can reflect the geometric distribution of the satellites participating in the precise single point positioning calculation. Generally, the smaller the position accuracy factor, the higher the positioning accuracy [30]. There are four time points in a day where PDOP undergoes significant mutations and the number of visible satellites decreases, indicating a relationship between

 doi:10.20944/preprints202505.1665.v1

PDOP and the number of visible satellites. Except for four time points during the day where there were significant mutations in PDOP, the PDOP values for all other time periods were less than 3.

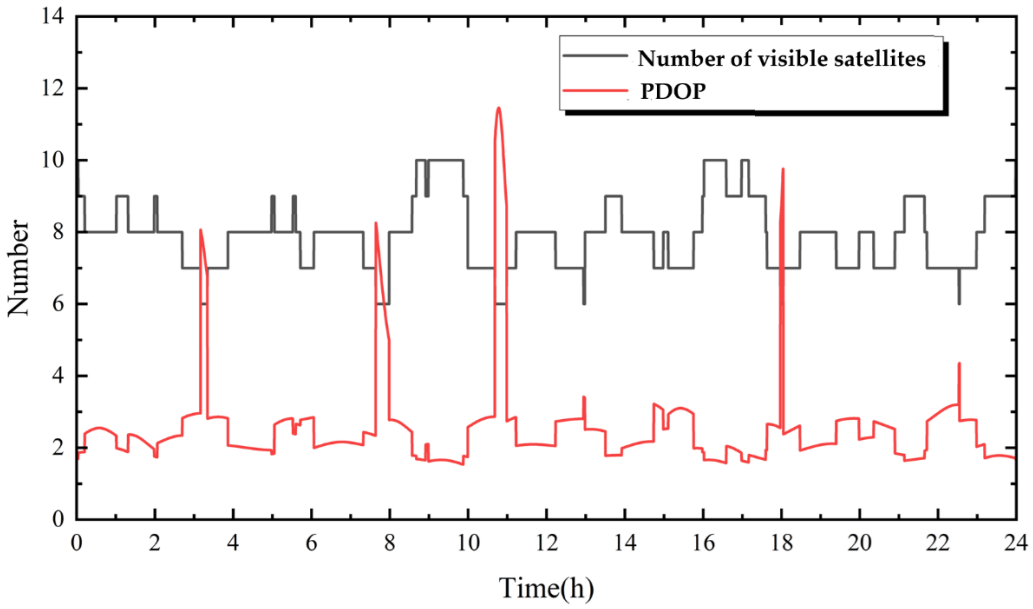

Figure 22. The number of visible satellites and PDOP during BDS-3 calculation at GAMG.

Table 8 shows the average RMS error values of the static BeiDou single system PPP-B2b E/N/U direction for 5 IGS stations from March 22 to March 28, 2024, for a total of 7 days. The RMS values of the coordinates can reflect the degree of difference between each point in the calculated coordinate set and the mean. In Table 8, the positioning errors RMS of C59-PPP-B2b and C61_PPP-B2b in the E direction are mostly concentrated between 1-3 cm, while the positioning errors RMS in the U direction are slightly worse than those in the E and N directions, mostly concentrated between 2 cm and 8 cm. From the perspective of positioning error RMS, the GAMG station has the best positioning effect. Due to the number of observation satellites, the USUD station has a gap in positioning accuracy compared to other stations.

The average RMS values of the static positioning error in the E/N/U direction of the BDS-3 system C59-PPP-B2b are 2.49/1.84/5.02 cm, respectively. The average RMS values of the static positioning error in the E/N/U direction of C59-PPP-B2b are 2.54/1.96/5.12 cm, respectively. Both C59-PPP-B2b and C61_PPP-B2b can achieve centimeter level static positioning, and the positioning accuracy of C59-PPP-B2b in all directions is slightly better than that of C61_PPP-B2b from the positioning results of these 7 days.

Table 8. BDS-3 Static positioning error RMS.

Station	C59_PPP-B2b			C61_PPP-B2b		
	E(cm)	N(cm)	U(cm)	E(cm)	N(cm)	U(cm)
GAMG	0.68	0.87	2.62	0.89	1.16	2.81
GUA1	2.53	0.88	1.93	2.31	0.84	1.92
JFNG	0.87	1.7	7.07	1.03	1.92	6.86
SHA1	2.72	2.05	4.98	2.51	2.04	5.23
USUD	5.66	3.72	8.51	5.99	3.86	8.81

4.2.2. BDS-3 PPP-B2b Kinematic Positioning

PPP-B2b kinematic positioning is a simulated dynamic processing method that uses static observation data but dynamic PPP model. It does not estimate coordinate parameters as constants

 doi:10.20944/preprints202505.1665.v1

like static PPP, but adds white noise and re performs PPP calculation on satellite observation data to achieve the static simulated dynamic calculation effect.

Kinematic positioning has expanded the application scope of precision single point positioning, enabling real-time high-precision positioning of mobile receivers in fields such as vehicle navigation, aircraft navigation, and mobile measurement. In kinematic positioning, by introducing motion models and filtering algorithms, precise single point positioning can consider the motion state of the receiver, thereby achieving continuous estimation of the receiver's position and velocity, providing more accurate and stable positioning results.

Taking GAMG station on March 22, 2024 as an example, Figures 23 and 24 show the results of kinematic positioning in the E/N/U direction over time. The error sequences of kinematic positioning in the E/N/U direction are C59-PPP-B2b and C61_PPP-B2b from top to bottom, respectively. In order to more intuitively show the convergence effect, the image omits the daily convergence process. The RMS of the E/N/U directional errors after kinematic positioning convergence of C59-PPP-B2b are calculated to be 7.21/7.33/12.44 cm, and the RMS of the E/N/U directional errors after kinematic positioning convergence of C61_PPP-B2b are 8.12/7.92/14.22 cm, respectively. GAMG stands at the dynamic PPP-B2b positioning convergence, and the positioning errors of C59-PPP-B2b and C61_PPP-B2b fluctuate within plus or minus 0.3 meters.

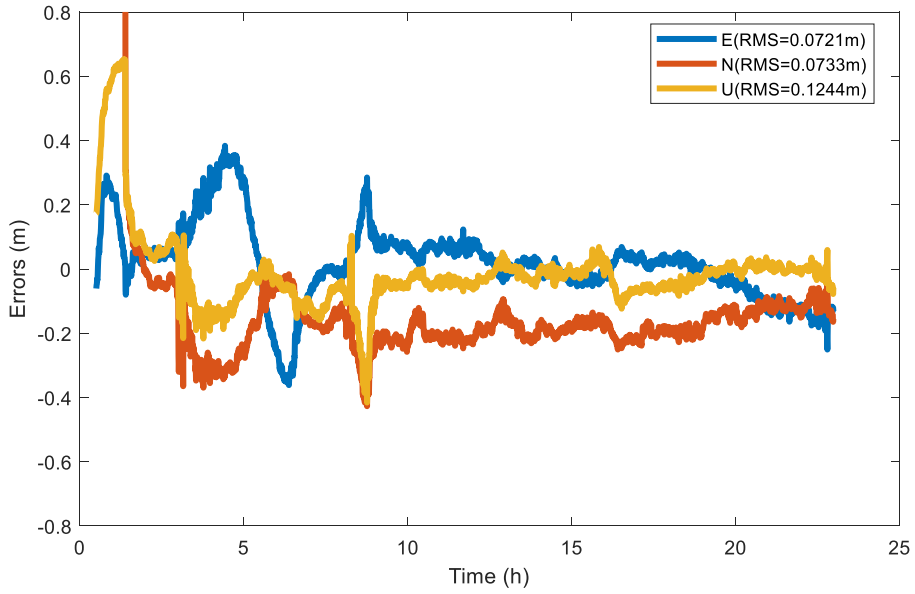

Figure 23. GAMG station C59_PPP-B2b kinematic positioning results.

 doi:10.20944/preprints202505.1665.v1

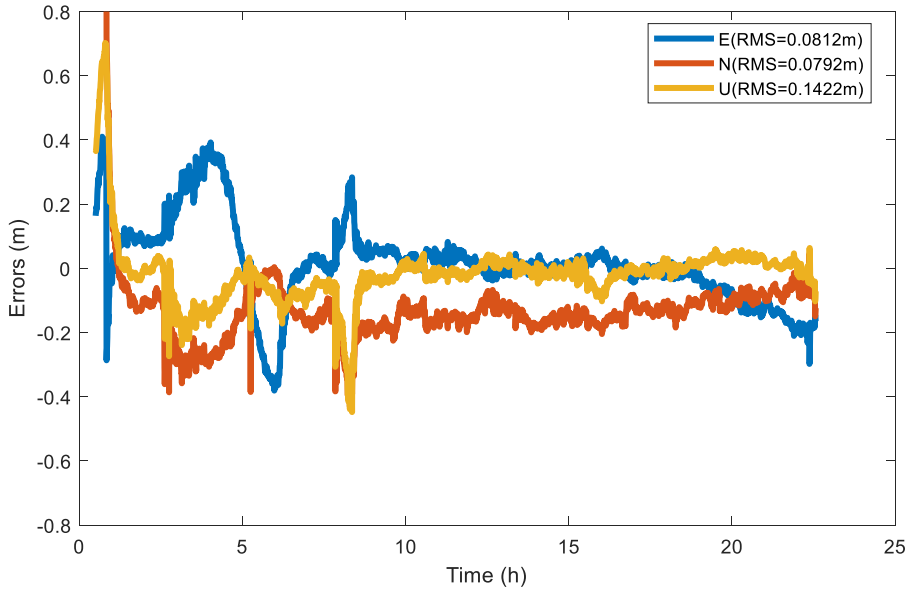

Figure 24. GAMG station C61_PPP-B2b kinematic positioning results.

Table 9 shows the average RMS error values of the dynamic single BeiDou PPP-B2b E/N/U direction for 5 IGS stations from March 22 to March 28, 2024, for a total of 7 days. In Table 9, the RMS errors of kinematic positioning of C59-PPP-B2b and C61_PPP-B2b in the E and N directions are mostly concentrated between 5 cm and 15 cm, while the RMS errors in the U direction are mostly concentrated between 15 cm and 25 cm, still slightly inferior to the RMS errors in the E and N directions.

The average RMS values of the kinematic positioning errors in the N/E/U direction of the BDS-3 system C59-PPP-B2b are 10.43/7.53/16.49 cm, respectively. The average RMS values of the kinematic positioning errors in the N/E/U direction of C61_PPP-B2b are 16.45/8.42/18.75 cm, respectively. In terms of positioning errors in different directions, C59-PPP-B2b and C61_PPP-B2b show high consistency between dynamic and static positioning.

Table 9. BDS-3 Kinematic positioning error RMS.

Station	C59_PPP-B2b			C61_PPP-B2b		
	E(cm)	N(cm)	U(cm)	E(cm)	N(cm)	U(cm)
GAMG	0.68	0.87	2.62	0.89	1.16	2.81
GUA1	2.53	0.88	1.93	2.31	0.84	1.92
JFNG	0.87	1.7	7.07	1.03	1.92	6.86
SHA1	2.72	2.05	4.98	2.51	2.04	5.23
USUD	5.66	3.72	8.51	5.99	3.86	8.81

5. Conclusions

For satellite orbit, PPP-B2b mainly corrects the orbital discontinuity caused by hourly updates of broadcast ephemeris, and also improves the orbit accuracy to a certain extent; For the clock bias of the BeiDou satellite, it not only corrected the hourly discontinuity in the broadcast ephemeris but also improved the accuracy. However, the PPP-B2b product did not improve the clock bias accuracy of GPS; For the real-time code deviation information carried in PPP-B2b, the deviation from the code deviation product released by the Chinese Academy of Sciences shall not exceed 2ns. Overall, PPP-B2b broadcasted by C59 has better correction effects on satellite orbit and clock bias than C61.

In terms of PPP-B2b time comparison, the zero baseline time comparison results fluctuate within the range of 0.5ns, STD is better than 0.1ns, and the frequency stability of 100000 seconds is better than 4E-16. In the long baseline time comparison, using the time comparison results of GBM products

 doi:10.20944/preprints202505.1665.v1

as a reference, the residual of C59_PPP-B2b time comparison fluctuates within 2ns, and the frequency stability reaches 3.87E-15 at 100000 seconds; The time comparison residual of C61_PPP-B2b also fluctuates within 2ns, with a frequency stability of 1.99E-15 at 100000 seconds. In the time comparison, C59_PPP-B2b and C61_PPP-B2b have similar accuracy, but C59_PPP-B2b has better usability and stability than C61_PPP-B2b.

When PPP-B2b is statically positioned, the average RMS values of errors in the N/E/U direction for C59-PPP-B2b and C61_PPP-B2b are 2.49/1.84/5.02 cm and 2.54/1.96/5.12 cm respectively. When dynamically positioned, the average RMS values of errors in the N/E/U direction for C59-PPP-B2b and C61_PPP-B2b are 10.43/7.53/16.49 cm and 16.45/8.42/18.75 cm respectively. Overall analysis shows that C59-PPP-B2b has better positioning performance than C61_PPP-B2b.

Author Contributions: Conceptualization, H.M. and J.Y.; methodology, H.W. and J.W.; software, J.Y.; validation, H.M. and H.W.; formal analysis, J.W.; investigation, H.M. and J.Y.; resources, H.W.; data curation, X.G.; writing—original draft preparation, J.Y. and H.M.; writing—review and editing, H.M. and J.Y.; visualization, X.G.; supervision, J.W.; project administration, H.W.; funding acquisition, H.W. All authors have read and agreed to the published version of the manuscript.

Funding: This research was financially supported by the Youth Innovation Promotion Association of the Chinese Academy of Sciences (No. Y2023109).

Data Availability Statement: The PPP-B2b data can be received by commercial receivers. The Observation data of IGS station can be downloaded at https://cddis.nasa.gov/Data_and_Derived_Products/GNSS/clock_products.html. The DCB data can be ftp://igs.igr.fr/pub/igs/products/mgex/dcb. The precise ephemeris data can be downloaded at http://www.ppp-wizard.net/products/REAL_TIME/.

Conflicts of Interest: The authors declare no conflicts of interest.

References

1. Tan, B.; Ai, Q.; Yuan, Y. Analysis of Precise Orbit Determination of BDS-3 MEO and IGSO Satellites Based on Several Dual-Frequency Measurement Combinations. *Remote Sensing* **2022**, *14*, 6030.
2. Yang, Y.; Liu, L.; Li, J.; Yang, Y.; Ren, X. Featured services and performance of BDS-3. *Science Bulletin* **2021**.
3. Zhao, Q.; Guo, J.; Liu, S.; Tao, J.; Hu, Z.; Chen, G. A variant of raw observation approach for BDS/GNSS precise point positioning with fast integer ambiguity resolution. *Satellite Navigation* **2021**, *2*, 29, doi:10.1186/s43020-021-00059-7.
4. de Oliveira, P.S.; Morel, L.; Fund, F.; Legros, R.; Monico, J.F.G.; Durand, S.; Durand, F. Modeling tropospheric wet delays with dense and sparse network configurations for PPP-RTK. *GPS Solutions* **2017**, *21*, 237-250, doi:10.1007/s10291-016-0518-0.
5. Goss, A.; Hernández-Pajares, M.; Schmidt, M.; Roma-Dollase, D.; Seitz, F. High-Resolution Ionosphere Corrections for Single-Frequency Positioning. *Remote Sensing* **2020**, *13*, 12.
6. CSNO. BeiDou Navigation Satellite System Signal In Space Interface Control Document Open Service Signal B2b (Version 1.0), China Satellite Navigation Office: Beijing, China, July, 2020. Available online: http://www.beidou.gov.cn/xt/gfxz/202008/P020230516558683155109.pdf (accessed on
7. CSNO. BeiDou Navigation Satellite System Signal In Space Interface Control Document Precise Point Positioning Service Signal PPP-B2b (Version 1.0), China Satellite Navigation Office: Beijing, China, July, 2020. Available online: http://www.beidou.gov.cn/xt/gfxz/202008/P020230516558683155109.pdf (accessed on
8. Tu, R.; Zhang, P.; Zhang, R.; Liu, J.; Lu, X. Modeling and performance analysis of precise time transfer based on BDS triple-frequency un-combined observations. *Journal of Geodesy* **2019**, *93*, 837-847, doi:10.1007/s00190-018-1206-3.
9. Yang, H.; Ren, X.; Liu, M.; Zhang, X. Dual-frequency to five-frequency real-time precise point positioning using new BDS-3 PPP-B2b service. *Earth, Planets and Space* **2024**, *76*, 82, doi:10.1186/s40623-024-02031-6.

 doi:10.20944/preprints202505.1665.v1

10. Zhang, P.; Tu, R.; Gao, Y.; Zhang, R.; Han, J. Performance of Galileo precise time and frequency transfer models using quad-frequency carrier phase observations. *GPS Solutions* **2020**, *24*, 40, doi:10.1007/s10291-020-0955-7.
11. Xu, W.; Yan, C.; Chen, J. Performance evaluation of BDS-2/BDS-3 combined precise time transfer with B1I/B2I/B3I/B1C/B2a five-frequency observations. *GPS Solutions* **2022**, *26*, 80, doi:10.1007/s10291-022-01262-y.
12. Ge, Y.; Zhou, F.; Liu, T.; Qin, W.; Wang, S.; Yang, X. Enhancing real-time precise point positioning time and frequency transfer with receiver clock modeling. *GPS Solutions* **2018**, *23*, 20, doi:10.1007/s10291-018-0814-y.
13. Kazmierski, K.; Zajdel, R.; Sośnica, K. Evolution of orbit and clock quality for real-time multi-GNSS solutions. *GPS Solutions* **2020**, *24*, 111, doi:10.1007/s10291-020-01026-6.
14. Ge, Y.; Dai, P.; Qin, W.; Yang, X.; Zhou, F.; Wang, S.; Zhao, X. Performance of Multi-GNSS Precise Point Positioning Time and Frequency Transfer with Clock Modeling. *Remote Sensing* **2019**, *11*.
15. Wang, L.; Li, Z.; Ge, M.; Neitzel, F.; Wang, Z.; Yuan, H. Validation and Assessment of Multi-GNSS Real-Time Precise Point Positioning in Simulated Kinematic Mode Using IGS Real-Time Service. *Remote Sensing* **2018**, *10*, 337.
16. Wang, S.L.; Ge, Y.L.; Meng, X.L.; Shen, P.L.; Wang, K.D.; Ke, F.Y. Modelling and Assessment of Single-Frequency PPP Time Transfer with BDS-3 B1I and B1C Observations. *REMOTE SENSING* **2022**, *14*, doi:10.3390/rs14051146.
17. Tao, J.; Liu, J.; Hu, Z.; Zhao, Q.; Chen, G.; Ju, B. Initial Assessment of the BDS-3 PPP-B2b RTS compared with the CNES RTS. *GPS Solutions* **2021**, *25*, 131, doi:10.1007/s10291-021-01168-1.
18. Sun, S.; Wang, M.; Liu, C.; Meng, X.; Ji, R. Long-term performance analysis of BDS-3 precise point positioning (PPP-B2b) service. *GPS Solutions* **2023**, *27*, 69, doi:10.1007/s10291-023-01409-5.
19. Ren, Z.; Gong, H.; Peng, J.; Tang, C.; Huang, X.; Sun, G. Performance assessment of real-time precise point positioning using BDS PPP-B2b service signal. *Advances in Space Research* **2021**, *68*, 3242-3254, doi:https://doi.org/10.1016/j.asr.2021.06.006.
20. Zhang, R.; He, Z.; Ma, L.; Xiao, G.; Guang, W.; Ge, Y.; Zhang, X.; Zhang, J.; Tang, J.; Li, X. Analysis of BDS-3 PPP-B2b Positioning and Time Transfer Service. *Remote Sensing* **2022**, *14*, doi:10.3390/rs14122769.
21. Nie, Z.; Xu, X.; Wang, Z.; Du, J. Initial Assessment of BDS PPP-B2b Service: Precision of Orbit and Clock Corrections, and PPP Performance. *Remote Sensing* **2021**, *13*, doi:10.3390/rs13112050.
22. Dai, W.; Liu, N.; Zhang, Z.; Tang, C.; Zhang, Z.; Yang, Y.; Pan, L. BDS-3/GPS uncombined real-time PPP with PPP-B2b precise products: Modeling and its long-term performance evaluation. *Advances in Space Research* **2025**, *75*, 7212-7225, doi:https://doi.org/10.1016/j.asr.2025.03.005.
23. CSNO. BeiDou Navigation Satellite System Signal In Space Interface Control Document Open Service Signal B1I (Version 3.0), China Satellite Navigation Office: Beijing, China, February, 2019. Available online: http://www.beidou.gov.cn/xt/gfxz/201902/P020190227593621142475.pdf (accessed on
24. CSNO. BeiDou Navigation Satellite System Signal In Space Interface Control Document Open Service Signal B3I (Version 1.0), China Satellite Navigation Office: Beijing, China, February, 2018. Available online: http://www.beidou.gov.cn/xt/gfxz/201802/P020180209623601401189.pdf (accessed on
25. Tang, J.; Lyu, D.; Zeng, F.; Ge, Y.; Zhang, R. Modelling and Assessment of BDS-3 Real-time Precise Point Positioning Time Transfer Based on PPP-B2b Service. *Mathematical Problems in Engineering* **2022**, *2022*, 4054179, doi:https://doi.org/10.1155/2022/4054179.
26. Liu, Y.; Yang, C.; Zhang, M. Comprehensive Analyses of PPP-B2b Performance in China and Surrounding Areas. *Remote Sensing* **2022**, *14*, doi:10.3390/rs14030643.
27. CSNO. BeiDou Navigation Satellite System Signal in Space Interface Control Document Open Service Signal B1C (Version 1.0); ChinaSatellite Navigation Office: Beijing, China, December, 2017. Available online: http://www.beidou.gov.cn/xt/gfxz/201712/P020171226741342013031.pdf (accessed on
28. Xu, Y.; Yang, Y.; Li, J. Performance evaluation of BDS-3 PPP-B2b precise point positioning service. *GPS Solutions* **2021**, *25*, 142, doi:10.1007/s10291-021-01175-2.
29. NTSCCAS. National Time Service Center of the Chinese Academy of Sciences, Global ground station GPS navigation information data (Jilin Station). 1.0. National Space Science Data Center.

 doi:10.20944/preprints202505.1665.v1

30. Yang, Y.; Li, J.; Xu, J.; Tang, J. Generalised DOPs with Consideration of the Influence Function of Signal-in-Space Errors. *Journal of Navigation* **2011**, *64*, S3-S18, doi:10.1017/S0373463311000415.